ARTICLE

Multilayer Self-Assembly of TiO_2 Nanoparticles and Polyaniline-*Grafted*-Chitosan Copolymer (CPANI) for Photocatalysis

Debajyoti Mahanta, Uttam Manna, Giridhar Madras, and Satish Patil*

Solid State and Structural Chemistry Unit, Institute of Science, Bangalore, India, 560012

ABSTRACT A photocatalytic thin film of TiO_2 nanoparticles and polyaniline-*grafted*-chitosan (CPANI) was fabricated by layer-by-layer (LbL) approach. The growth of the self-assembly of polymer nanocomposite was monitored by UV−vis spectroscopy and the thin film morphology was analyzed from scanning electron microscopy (SEM). Poly(styrene sulfonate) (PSS) was used as a bridging layer between TiO_2 nanoparticles and CPANI. Incorporation of CPANI within the LbL self-assembly of polymer nanocomposites enhanced the dye degradation ability of the thin film. These results indicate that the presence of CPANI improves the adsorption of dye in the self-assembly. The effect of surface area and the amount of catalyst was also examined. The reusability of the thin films for dye degradation study ensures the stability of the self-assembly.

KEYWORDS: layer-by-layer • chitosan • polyaniline • TiO_2 nanoparticles • dye degradation

INTRODUCTION

One of the major source of water contamination is the textile dyes produced in various textile industries (1). During the past decade, photodegradation (2−4) have been extensively pursued for effective removal of textile dyes from wastewater. Although various other methods such as adsorption of dyes by various adsorbents (5−7), reverse osmosis (8), flocculation (9), etc. are employed for the wastewater treatment. Among all these methods, photodegradation is the most widely studied method for the purification of water. Recently, our group has found that **PANI** is also efficient for selective adsorption of the dyes through chemical interaction (10, 11). For photodegradation, TiO_2 nanoparticles have been the most promising and well-studied material as an efficient photocatalyst because of favorable band gap, large surface area and nontoxicity (12). Generally, TiO_2 nanoparticles are dispersed in the contaminated dye solution and the heterogeneous photocatalytic degradation reactions occur on the surface of the TiO_2 nanoparticles. The advantage of this method is that, the maximum surface area of the catalyst is exposed to the solution for heterogeneous photocatalytic reactions but the limitation is the separation of the catalyst from the reaction media and recombination of photogenerated electron hole pair.

Promising new methods have been proposed for efficient separation of catalysts (13−15). One proposed method is the preparation of polymer nanocomposite thin films. In this approach, the catalyst can be separated from the reaction medium just by taking out the thin films from the solution. Among several film forming methods, such as spin coating, drop casting, dip coating etc., the layer-by-layer (LbL) approach is one of the simplest and promising method to fabricate a thin film with desired properties (16). Decher et al. introduced this unique approach based on electrostatic interaction between two complementary polyelectrolyte solution (17). Varieties of materials (18−22) (polyelectrolyte, neutral polymer, micells, dendrimers, nanoparticles, etc.) have brought into the multilayer assembly by using this simple LbL approach through electrostatic interaction (23), hydrogen bonding (24), and covalent bonding (25). Different techniques have been used for the fabrication of thin films of TiO_2 nanoparticles (26). A porous and stable thin film that was prepared from LbL approach was first reported by He et al. (27) Subsequently, extensive studies on the morphology and porosity of this assembly was carried out by Kniprath et al. (28) This porous multilayer assembly of TiO_2 and poly(styrene sulfonate) (**PSS**) shows better photocatalytic activity than TiO_2 film that are prepared from other techniques (29).

Rubner and co-workers fabricated multilayer assembly of polyaniline (**PANI**) with both ionic and nonionic polymer through electrostatic and hydrogen bonding, respectively, where the content of polyaniline was higher within the assembly for hydrogen bonded systems (30, 31).

In this report, we demonstrate the photocatalytic activity of multilayer porous thin film of TiO_2 nanoparticles by bridging polyaniline-*grafted*-chitosan (CPANI) and PSS. Unlike previous studies, PSS was dissolved in distilled water at neutral pH, it has negative charge, whereas CPANI and TiO_2 nanoparticles are positively charged at pH 3 (in acetic acid

* To whom correspondence should be addressed. Tel: +91-80- 22932651. Fax: +91-80-23601310. E-mail: satish@sscu.iisc.ernet.in.

Received for review September 27, 2010 and accepted November 24, 2010

DOI: 10.1021/am1009265

Published on Web 12/09/2010

solution). Thus in these films, each CPANI and TiO_2 layers were sandwiched in between two PSS layers, which bridges the CPANI and TiO_2 layers. The incorporation of **CPANI** within the multilayer assembly of TiO_2 nanoparticle was motivated from dye adsorption property of both chitosan (32) and polyaniline (10, 11). PANI can not be used directly to perform LBL deposition because it is not soluble in water and a majority of the organic solvents. However, when PANI is grafted on chitosan, it is soluble in aqueous solutions at acidic pH. Here, it acts as a positively charged polyelectrolyte allowing **CPANI** to form multilayer films.

Thus, in our approach, adsorption of dye molecules by **CPANI** increases the photocatalytic activity by bringing more and more dye molecules in proximity of TiO_2 nanoparticles within this multilayer thin film. Further, we show that the film is stable and retains its activity.

EXPERIMENTAL SECTION

Materials. Aniline (SD. Fine Chem. Ltd., India) was purified by double distillation before use. Ammonium persulphate (APS), hydrochloric acid, Orange G (OC), Rhodamine B (RB), glacial acetic acid, *N*-methyl-2-pyrrolidone (NMP), acetone, and methanol (AR grade) were bought from SD Fine Chem. Ltd., India and used without any further purification. Chitosan of average molecular weight $M_w \approx 120\,000$ and poly(styrene sulfonate) sodium salt (PSS), $M_w = 70\,000$ were obtained from Sigma Aldrich and used without any further purification. Ultrapure (Millipore) water with specific resistance 18.2 MΩ cm was used in all experiments.

Scheme 1. Synthesis of Polyaniline-*Grafted*-Chitosan (CPANI)

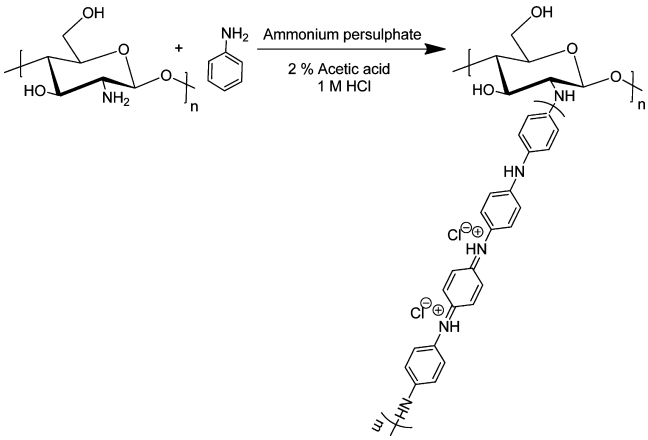

Chitosan was completely dissolved in 2 wt % acetic acid by stirring for 2 h on a magnetic stirrer. Aniline and 1 M HCl were mixed in a separate beaker and added to the chitosan solution at 5 °C, with constant stirring. Then the polymerization was carried out by the slow addition of APS at 0−5 °C as described by MacDiarmid et al. (33). Stirring was continued in an ice bath at temperature 0−5 °C for 6 h. Following this reaction, the final reaction mixture was neutralized by addition of 1 M NH_4OH solution. The product was precipitated in neutral medium. The product was then separated by centrifugation followed by washing with Millipore water to separate unreacted APS, HCl, NH_4Cl. The washed product was separated and again washed with *N*-methyl-2-pyrrolidone (**NMP**) for several times to separate PANI. The product was finally washed with distilled water to remove the NMP from the product. The product was then dissolved in 2% acetic acid, and 1 M HCl was added to it and stirred for 12 h to get doped PANI chains in the grafted copolymer. The final grafted copolymer with doped PANI chains was separated by precipitation in a large volume of methanol. The final product was washed with methanol several times and dried under a vacuum for 12 h at room temperature.

Different samples of grafted copolymer were synthesized with different chitosan to aniline ratios defined by X/A as described by Yang et al. (34), which is the ratio of NH_2 groups on chitosan (X) to the number of aniline (A) molecules. In a typical reaction to prepare X/A = 1:3, 1 g of Chitosan was dissolved in 120 mL of 2 (weight%) acetic acid and stirred for 2 h to dissolve completely. Sixty milliliters of 3 M HCl was added to the chitosan solution to make the HCl concentration 1 M in the reaction media. Then 1.554 g aniline was added to the above mixture and stirred in an ice bath for 1 h to maintain the temperature within 0 to 5 °C. 0.876 g of APS was dissolved in 100 mL 1 M HCl and this solution was slowly added to the chitosan−aniline acidic mixture at 0 to 5 °C. The final product CPANI was separated and purified by the procedure explained above.

Solution Preparation. CPANI solution of concentration 1 mg/mL was prepared by dissolving 500 mg of **CPANI** in 4% acetic acid. The solution was stirred for overnight to dissolve **CPANI** completely. In another beaker 500 mg PSS was dissolved in 500 mL of Milli-Q water. Twenty-five milligrams of TiO_2 (P25) of average diameter 21 nm was dispersed in 500 mL of 4% acetic acid.

Preparation of Thin Film by LBL Approach. The glass slides of area 37 × 25 mm were taken as planar substrate for the layer-by-layer deposition of CPANI, PSS and TiO_2. The glass slides were cleaned and then kept in piranha solution for 12 h. It induces negative potential to the glass surface. The glass slides were washed with Millipore water several times. The glass slides with negatively charged surface were then dried with nitrogen flow. All the glass slides were then placed in the CPANI solution for 24 h to form the first layer of CPANI on the glass surface. The ionic interaction of the positively charged CPANI chains and the negatively charged glass substrate is the driving force for the adsorption of CPANI on the glass surfaces. The glass slides were then washed with Millipore water and dried under nitrogen flow. The slides were kept in PSS solution for 12 h for adsorption of negatively charged PSS polymer chains on the positively charged CPANI layer. After washing and drying, the slides were kept in the TiO_2 dispersed solution for 2 h to adsorb the TiO_2 particles (with positive surface charge) on the negatively charged PSS layer. Again, the slides were kept in PSS solution to form a layer of PSS on the top of TiO_2 layer. Thus, one TiO_2 layer is formed on the deposition of one tetra layer which is represented by (CPANI- PSS- TiO_2- PSS). Thus the cycle was repeated again and again to get the required number of multilayer deposition of TiO_2 and **CPANI** on the glass substrates. It should be noted that initially the density of charge on the surface is small, so the slides were kept for longer time for deposition of initial layers.

Degradation Studies. The photochemical reactor used in this study consists of a jacketed quartz tube of 3.4 cm inner diameter, 4 cm outer diameter, and 21 cm length. A high pressure mercury vapor lamp of 125 W (Philips, India) that radiated predominantly at 365 nm (3.4 eV) was placed inside the reactor after carefully removing the outer shell. Water was circulated through the annulus to avoid heating during the reaction. For all photo catalytic reactions, a 100 mL beaker was used and for all experiments 50 mL of dye solution was used for degradation. The required numbers of glass slides were placed vertically and a small magnetic pellet was used to stir the dye solution during the degradation reaction. In all the degradation reactions, the dye solution was kept at a distance of 15 cm from the light source. It was ensured that no degrada-

tion of the dyes was observed in the absence of either UV or the catalyst. Ice water was used to cool the source during all the kinetic experiments. 0.5 mL of dye solution was collected after different time intervals for kinetic study. The concentration of the dye solution was determined by UV−vis spectroscopy. The intensity was converted to concentration from a calibration curve using Beer−Lambert law.

Characterization. ***FTIR Spectroscopy.*** The dried samples were grounded with KBr powder and the mixtures were made into pellets under high pressure. FTIR spectra have been recorded on a Perkin-Elmer FT-IR spectrophotometer, spectrum 1000.

UV−Vis spectroscopy. The UV−vis spectra of multilayer films deposited on glass slides after deposition of different numbers of TiO_2 layers and the concentration of the dye solution during the degradation reaction were recorded with Perkin- Elmer (Lambda-35) spectrometer.

Scanning Electron Microscopy (SEM). The morphology of the films and the thickness of the films were determined by performing the SEM measurement using JEOL, JSM-5600LV scanning electron microscope at 5 kV.

RESULTS AND DISCUSSION

Characterization of CPANI. **CPANI** was prepared by following the reported procedure as shown in Scheme 1 in literature (34). The formation of CPANI was confirmed by FTIR, NMR, and UV−vis spectroscopy. Figure S1 in the Supporting Information shows the FTIR spectra of CPANI and chitosan (35). The distinctive chitosan bands were observed at 3413 cm^{-1} due to −OH vibration and the characteristic −CH stretching of chitosan was appeared at 2881 cm^{-1} (36). Skeletal vibration of C−O stretching for saccharide structure appeared at 1073 cm^{-1} (37). The characteristic bands of **PANI** appeared at 1572 and 1481 cm^{-1} which are attributed to C═C & C═N stretching of quinoid and benzenoid rings, respectively (38, 39). The bands at 1300 and 799 cm^{-1} correspond to para substituted aromatic ring and aromatic **C−N** stretching of PANI. Reduced intensity of native chitosan **C−H** stretching and characteristic bands of substituted polyaniline in **CPANI** spectra clearly indicates strong evidence of grafting. The grafting was further confirmed by NMR spectroscopy. The NMR of CPANI was recorded in DMSO- d_6 and a few drops of 1 M HCl were added to the solvent to dissolve CPANI. The doped CPANI gives a characteristic NMR peak at 7.25 ppm (see Figure S2 in the Supporting Information) due to grafting (40).

Figure 1 shows the UV−visible spectra of **CPANI** dissolved in aqueous solution of acetic acid. It was observed that at acidic pH, **CPANI** has all the characteristic peaks of doped polyanilne. A broad peak at around 837 nm is due to bipolaron transitions of grafted polyaniline on chitosan. A shoulder peak at 430 nm is due to semiquinone, and the peak at 350 nm is due to π to π^* transition (41). These results suggest that the optical properties of grafted polyaniline on chitosan remain unaffected. We have also found the shift of the peak ~835 nm on addition of HCl into the CPANI solution (in 2% acetic acid) as shown in Figure 1. So, from the UV−visible spectra, it is examined that we can tune the dopant levels by treating with weak or strong acidic media as a solvent for the CPANI. The pK_a value of chitosan is

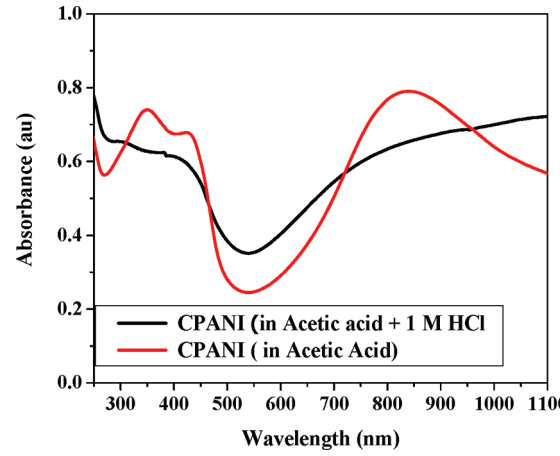

FIGURE 1. UV−vis spectra of polyaniline-*grafted*-chitosan copolymer (CPANI) in 2 wt % acetic acid and in a mixture of acetic acid and 1 M HCl solutions.

around 6.5 (42). There is a competition between the PANI side chains and the amine moieties on chitosan to consume HCl. Thus, the amine moieties on the chitosan backbone prevent the complete doping of **PANI** side chains during the doping process in 1 M HCl (as discussed in experimental section). This tuning of doping level and hydrophilic environment around PANI moiety encouraged us to build a multilayer self-assembly of CPANI and TiO_2 nanoparticles via LbL approach and apply it for dye degradation.

Multilayer Thin Film. Layer-by-layer self-assembly of CPANI and TiO_2 nanoparticles through electrostatic interaction was monitored by UV−vis spectra as shown in Figure 2a. Negatively charged PSS was brought into this multilayer self-assembly as it has complementary potential to both CPANI and TiO_2. The UV−vis spectra of the film were recorded after deposition of each TiO_2 layer. The combined signature of both CPANI and TiO_2 has appeared at near 300 nm and this combined signature is increased with the number of layer deposition. It is hard to distinguish the spectral signature separately for CPANI and TiO_2 nanoparticle at this spectral region, TiO_2 nanoparticle has a broad signature and it overlaps with the UV−vis spectral signature of CPANI.

However, the regular increments of the broad peak at around 800 nm of CPANI (due to PANI moiety) on deposition of each CPANI-PSS-TiO_2 layer clearly indicates the growth of a multilayer thin film, as shown in inset of Figure 2a. This broad peak near 800 nm is thought to be due to trapped excitons centered on quinoid moieties of the polyaniline side chains present in CPANI. Thus, it reveals the layer-by-layer incorporation of both CPANI and TiO_2 nanoparticle within this multilayer thin film. Photograph of this multilayer thin film deposited on a quartz plate is shown in Figure 2b. The whitish green color of the film again confirms the presence of CPANI in the multilayer thin film. The thickness of this multilayer thin film was 1.5 ± 0.1 μm that was determined by the cross-sectional SEM image of the multilayer thin film having 20 numbers of TiO_2 layers. Uniform deposition of this multilayer thin film was also observed from cross sectional FESEM image of Figure 2c. Presence of TiO_2 nanoparticles

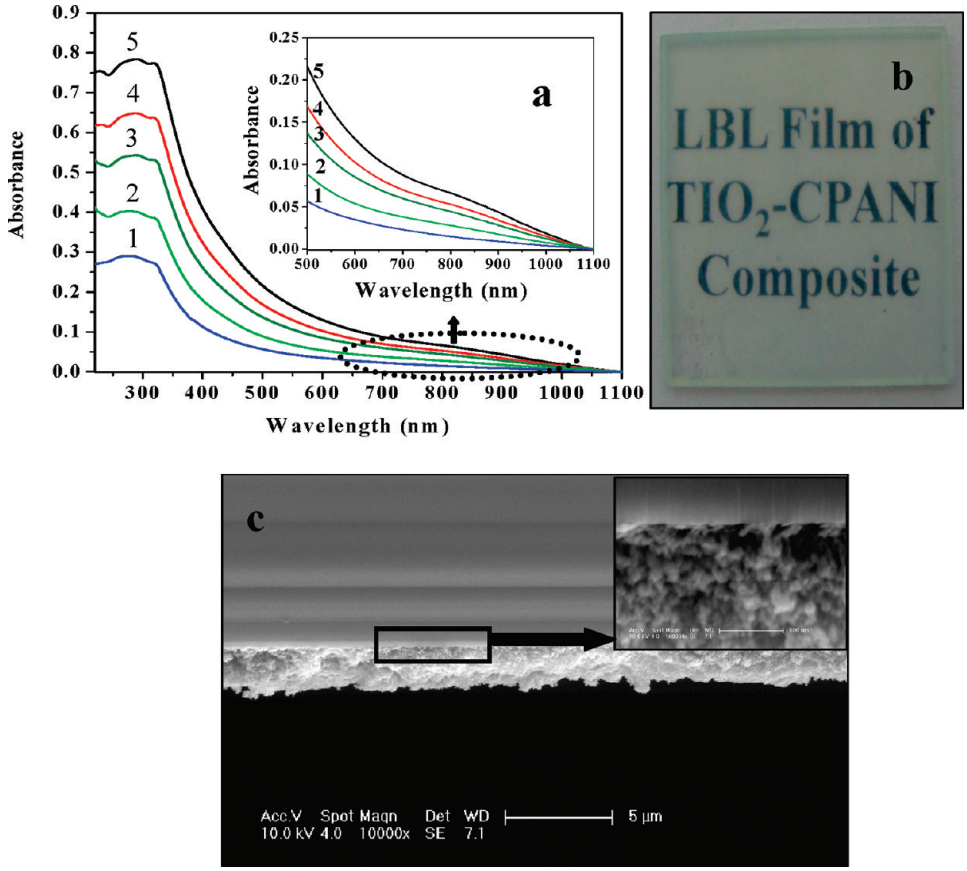

FIGURE 2. Layer-by-layer deposition of TiO_2 nano particle and CPANI by placing PSS in between them. (a) UV−vis spectra of LbL growth of this multilayer assembly where each spectrum was taken after TiO_2 deposition and inset shows signature of polyaniline moiety. (b) Photograph of the multilayer thin film of CPANI and TiO_2 on quartz plate. (c) Cross-sectional FESEM image of this multilayer thin film; the inset represents magnified image of this assembly.

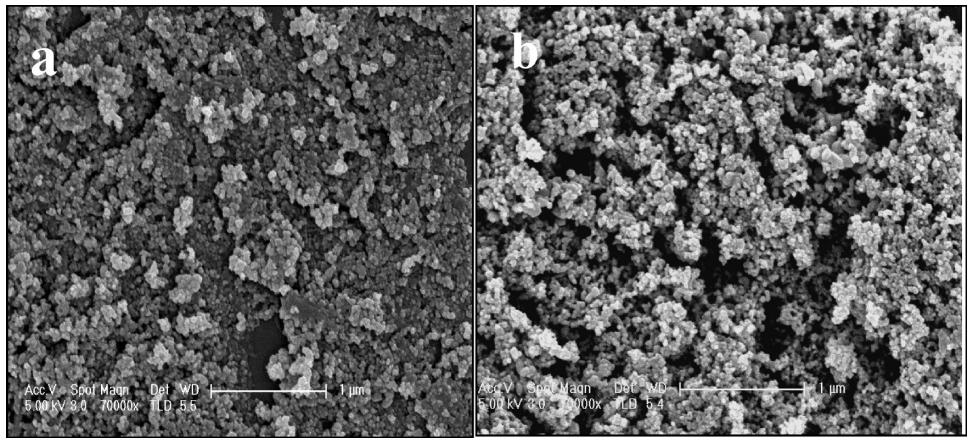

FIGURE 3. Morphology study of the LbL film of CPANI and TiO_2 nanoparticles. Morphology of multilayer thin film after deposition of (a) 3 and (b) 5 layers of TiO_2 nanoparticle, respectively.

within this multilayer thin film was clearly observed in the inset image of Figure 2c.

Film Morphology. The formation of the multilayer thin film and its morphological change with number of layer deposition of TiO_2 was again characterized under field emission scanning electron microscope (FESEM) as shown in Figure 3. The FESEM images of the multilayer thin films having 3 and 5 layers of TiO_2 nanoparticles are shown in images a and b in Figure 3, respectively. TiO_2 nanoparticles are clearly visible on the surface of this multilayer thin film as shown in corresponding images. Both the thin films are porous in nature, which helps to enhance the dye degradation efficiency of the film as discussed later.

Degradation Studies. In the degradation studies, we have used both orange G (**OG**) and rhodamine B (**RB**) as model dyes representing both the anionic and cationic class of dyes, respectively. We have performed control experiments for both the dyes using multilayer thin films of

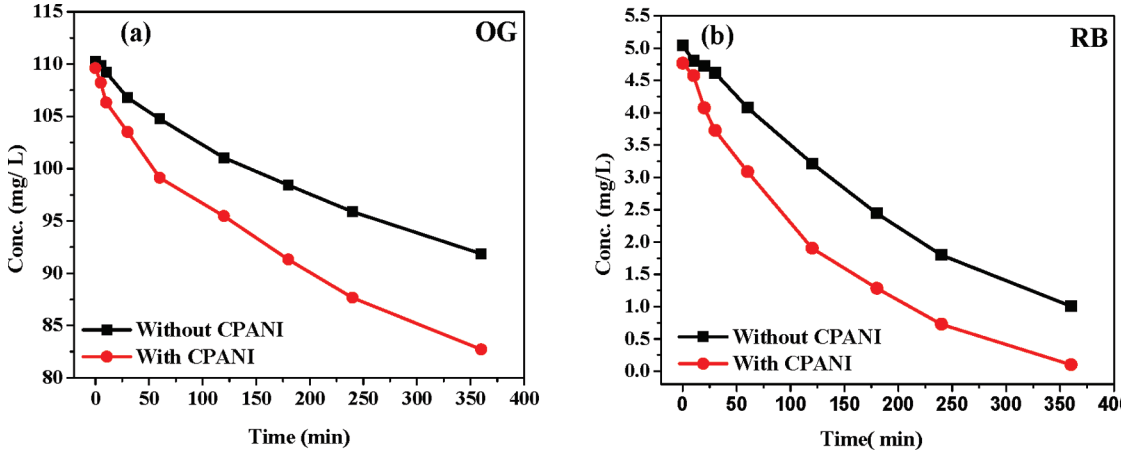

FIGURE 4. Degradation profile of (a) Orange G and (b) Rhodamine B in presence of catalytic slides with (red) and without (black) CPANI layers. All the films have five TiO_2 nanoparticles layers.

Table 1. Values of Degradation Efficiency, First-Order Rate Constant (k_0) and Regression Coefficient (R^2) for Degradation Studies of Orange G and Rhodamine B Carried out under Different Operating Conditions

params	operating conditions	η (%)	k_0 ($\times 10^{-3}$ min^{-1})	R^2
catalyst composition (OG)	without CPANI	16.69	0.56	0.977
	with CPANI	24.53	0.89	0.961
catalyst composition (RB)	without CPANI	80.01	4.33	0.996
	with CPANI	97.83	9.32	0.969
no. of TiO_2 layers (OG)	5	24.53	0.89	0.96
	10	36.12	1.36	0.981
	15	44.26	1.78	0.969
	20	57.39	2.5	0.992
no. of TiO_2 layers (RB)	5	32.07	1.06	0.99
	10	37.72	1.48	0.97
	15	54.46	2.17	0.998
	20	71.75	3.48	0.997
initial concentration (OG) (mg/L)	57.67	79.93	4.12	0.987
	85.45	61.96	2.74	0.991
	108.1	57.39	2.5	0.992
initial concentration (RB) (mg/L)	4.75	99.23	15.2	0.978
	9.79	99.13	7.36	0.997
	14.41	71.96	3.48	0.997
no. of slides (OG)	1	21.74	0.87	0.90
	2	29.15	1.13	0.886
	3	48.54	2.06	0.983
	4	57.39	2.5	0.992
no. of slides (RB)	1	31.41	1.21	0.936
	2	43.11	1.71	0.984
	3	55.37	2.31	0.991
	4	71.75	3.48	0.997

composition (CPANI- $PSS)_{10}$. No significant degradation was observed for both the dyes after performing the reaction for 6 h under UV/vis light.

This confirms that both the polyelectrolytes used in the multilayer film formation do not work as photocatalysts. Experiment were carried out for each dye to measure dye degradation behavior where two different thin films of TiO_2 nanoparticles were fabricated with two different compositions (one with PSS/TiO_2 and another with PSS/TiO_2/CPANI) and the degradation profiles of orange G (OG) and rhodamine B (RB) dye molecules by both the multilayer thin films are given in Figure 4. To perform all these experiments, we used 4 catalytic slides having 5 TiO_2 layers in each case. The CPANI containing films degrade the OG dye and RB dye molecules by ~1.6 and ~2.2 times faster respectively (details given in table 1) than PSS/TiO_2 multilayer thin film as noticed from above-mentioned control experiments. The better activities of the CPANI containing films can be explained based on the following facts: (i) the adsorption of dye molecules within the multilayer self-assembly is enhanced due to the presence of CPANI, as it contains both chitosan backbone and PANI side chains. Emeraldine salt of PANI adsorbs the anionic dyes (10, 11) and in its undoped state adsorbs the cationic dyes (43, 44).

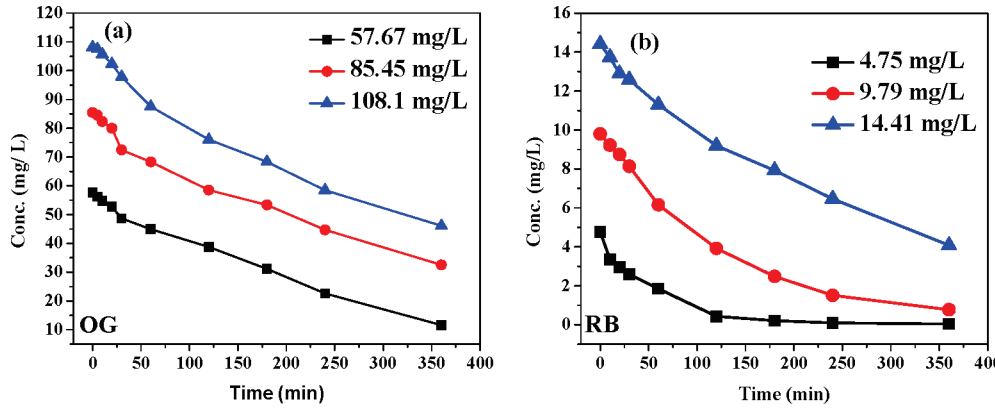

FIGURE 5. (a, b) Degradation profiles of Orange G (OG) and Rhodamine B (RB), respectively. Experiments are carried out with different initial concentrations and with same number of catalytic slides with same composition of (CPANI/PSS/TiO_2).

The PANI side chains of CPANI were doped by treating with 1 M HCl. But, some of the repeating units of PANI remain in the undoped state. Therefore, the doped portion of CPANI is responsible for adsorption of anionic dyes and undoped portion is responsible for cationic dyes. Thus, CPANI layers acts as an additional driving force to bring more dye molecules in the vicinity of the TiO_2 nanoparticle surfaces within the multilayer self-assembly and more dye degradation has taken place. (ii) CPANI can act as sensitizer for TiO_2 to show better photocatalytic activity due to presence of PANI side chains (45). (iii) Another important fact is that although both sets of catalytic slides, with and without CPANI layers, contain the same number of TiO_2 layers, they do not have the same number of PSS layers. The catalytic slides with CPANI contain double the number of PSS layers than that without CPANI containing catalytic slides. Thus, more number of negatively charged PSS layers may also be responsible for enhanced cationic dye adsorption on the CPANI containing catalytic slides. (iv) Porosity of the multilayer thin film is also responsible for better degradation of dye molecules by faster diffusion of it within the self-assembly.

The degradation of OG and RB molecules with different initial concentrations was performed to estimate the dye degradation capability of this multilayer thin film, as shown in Figure 5. In this set of experiments, four slides each of with 20 layers of TiO_2 nanoparticles were used for dye degradation study. It was observed that when the initial concentration of OG is 57.6 mg/L, the degradation is about 80% and it gets reduced to ~77 and ~62% for initial concentration of 108 and 85.5 mg/L respectively. The same trend is observed for the cationic dye Rhodamine B (RB) also but with much lower initial concentrations of dye. So, dye degradation by this multilayer assembly for a given layers of TiO_2 nanoparticles is restricted above certain concentration of the dye solutions.

To examine the role of the TiO_2 nanoparticle layer within this multilayer assembly on degradation of Orange G and Rhodamine B molecules, photocatalytic degradation reactions were performed in presence of fixed number (four) of catalytic slides (multilayer thin film from CPANI, PSS, and TiO_2 nanoparticles on microscopic glass slide) having different layers of TiO_2 nanoparticles. In all the experiments, four slides were used to maintain the constant surface area of the multilayer assembly, although the effective catalytic surface areas were different because of the difference in the number of TiO_2 layers. With an increase in number of layers, the amount of TiO_2 nanoparticles also increases in the catalytic films. As a result, the degradation rate was found to be increasing with the number of TiO_2 layers (as shown in Figure S3, see the Supporting Information). Thus, increasing the amount of TiO_2 nanoparticles enhances the catalytic activity of the films more. This is due to the porous nature of the multilayer films where dye molecules can easily diffuse within it to reach the surface of inner TiO_2 layers. To increase the capability of dye degradation, we have carried out a set of dye degradation experiments with different numbers of slides but keeping 20 layers of TiO_2 nanoparticles within each multilayer assembly.

An increase in the rate of degradation of both the dyes was observed when the number of slides in the container was increased (Figure S4, see the Supporting Information). Because the films are porous, the dyes can diffuse through the film and more dye is adsorbed by the films with CPANI and a thick film will adsorb more dye and results in faster degradation, as observed in a previous study (27). However, in our case, the increase in the value of k_0 is not linear with the number of slides used (Table 1). This indicates that **CPANI** plays an important role in degradation. Further, with an increase in number of slides, the exposed surface area of TiO_2 nanoparticles is increased in the reaction media (beaker) and more dye molecules get degraded. Thus the rate of degradation increases with number of catalytic slides for both the dyes.

Thus we can enhance the dye degradation capability of TiO_2 nanoparticles either by increasing the number of TiO_2 nanoparticle layer within the multilayer assembly or the number of catalytic slides in degradation reaction mixture,

Reusability of the Catalyst. The most important factor for the practical utility of a catalyst is its reusability and stability during the course of reactions. The reusability of the catalyst was studied by performing photocatalytic degradation reactions with the same set of slides for several cycles for both the dyes.

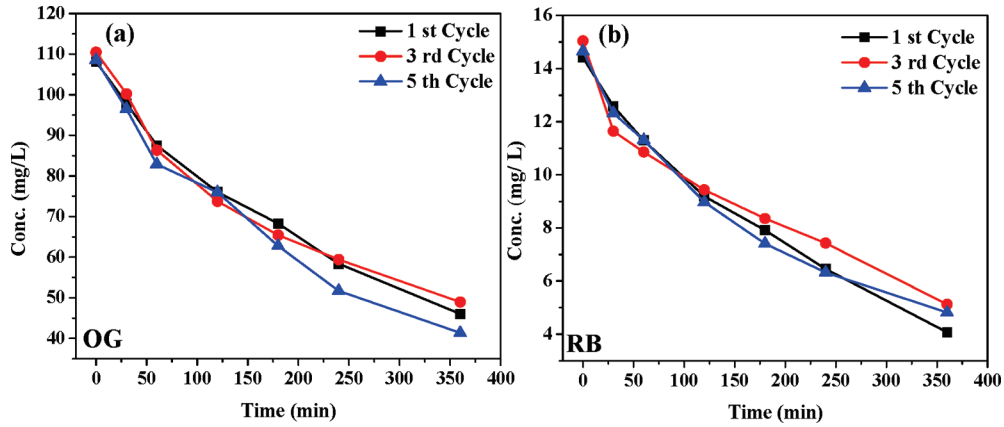

FIGURE 6. Reusability of the multilayer thin films. (a, b) Degradation profiles of OG and RB dye with same set of catalytic slides at different cycles.

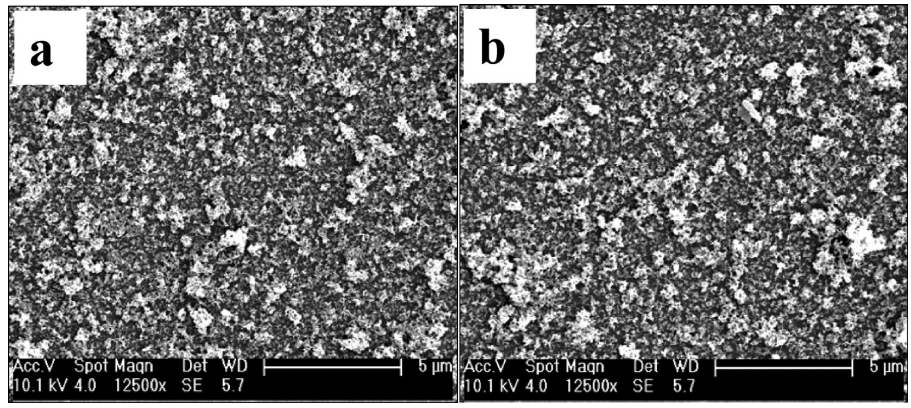

FIGURE 7. (a, b) SEM images of catalytic films before and after the photocatalytic degradation reaction of RB, respectively.

The stability of the multilayer thin films prepared by LbL technique was confirmed from studying the morphology of the film with FESEM before and after the photocatalytic degradation reactions. The degradations of OG and RB molecules were performed with 50 mL of each solution where initial concentrations were 100 ppm and 15 ppm respectively in the presence of same catalytic slides. It is observed that there is not much change in degradation profiles of both the dye solutions, as shown in Figure 6. The slight difference in degradation may be due to minor variation in the orientation of slides in each set of degradation reactions. This reusable behavior was observed due to strong layer-by-layer integrity of this multilayer thin film as the morphology of the film remains very much similar before and after 6 h degradation reactions as shown in Figure 7. From the morphology, it is clear that there is no noticeable morphological change after the degradation reactions. This stability ensures that the technique is robust for making TiO_2 thin films.

Kinetic Studies. The degradation efficiency of the dye is expressed by the equation

$$\eta\,\% = \frac{C_0 - C_t}{C_0} \times 100\,\%$$

Where C_0 is the initial concentration of the solution and C_t is the concentration of the dye solution at time t. For all the degradation experiments, the degradation coefficient after 6 h exposure under UV light is summarized in Table 1. To quantify the degradation reaction of dyes Orange G and Rhodamine B with the heterogeneous catalyst (CPANI-PSS-TiO_2-PSS)$_n$ LbL multilayer films, we used the following kinetic model. Heterogeneous photocatalytic reactions generally follow the Langmuir–Hinshelwood (L–H) kinetics

$$r_0 = \frac{k_0 C_0}{1 + K_0 C_0}$$

Where r_0 is the initial rate, k_0 is the kinetic rate constant, and K_0 is the adsorption coefficient of the reactant dye. As the value of C_0 is small, $K_0C_0 \ll 1$ and the L–H rate expression reduces to first-order rate expression

$$r_0 = \frac{dC_0}{dt} = k_0 C_0$$

This equation can be solved to obtain

$$\ln\left(\frac{C}{C_0}\right) = -k_0 t$$

In Figure 8, the plot of $-\ln(C/C_0)$ with time is shown for all sets of degradation reactions, from which the first-order rate

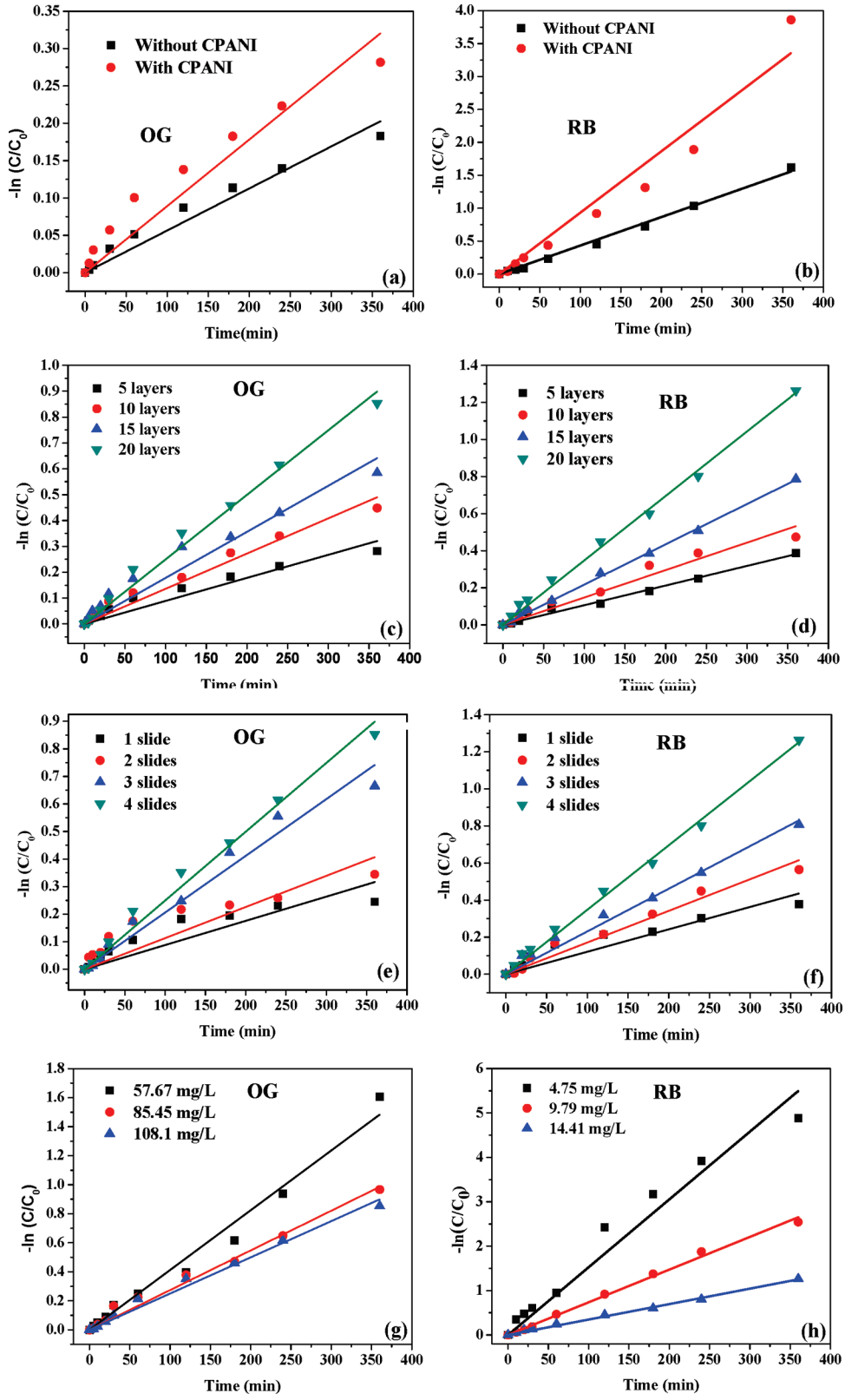

FIGURE 8. First-order kinetic plot of $-\ln(C/C_0)$ vs time (t) for photocatalytic degradation reactions (a, b) with and without CPANI layers in the catalytic slides, (c, d) with catalytic slides containing different number of TiO_2 layers, (e, f) with different number of catalytic slides, and (g, h) with different initial dye concentrations.

constant k_0 values of all degradation reactions are determined. The rate constant values for all the degradation reactions are summarized in Table 1.

Table 1 summarizes the degradation efficiency η %, first-order rate constant k_0, and regression coefficient for the degradation studies, carried under different operational

conditions. We observed that the first-order rate constant value for the degradation of both the dyes increases with the increase in number of TiO_2 layers. This indicates that the porosity of the films prepared by LBL approach allows the dye molecules to diffuse through and reach the TiO_2 surfaces. Thus the amount of the catalyst and hence effective surface area for the photocatalytic degradation reaction increases with the increase in the number of TiO_2 layers, although the number of catalytic slides remains constant in all the cases. It is seen from the Table 1 that the first-order rate constant value also increases with increase in the surface area of the catalyst. However, the increase in degradation rate is not linear with increase in the number of layers. Though the degradation of dye can occur at both the inner and outer layer of the catalyst, the efficiency of TiO_2 in the inner layer is lesser than the upper layer (29). As the number of layer increases, the diffusion of the dye in and out of the layers plays an important role in the kinetics. The other observation is that both the % of degradation after 6 h and the first-order rate constant values decrease with the increase in initial concentration for both the dyes. This is due to two reasons (29): (a) the light intensity reaching the TiO_2 is reduced because of the lower transparency of the solution at higher concentrations and (b) more organic substances are adsorbed on to the surface of TiO_2 at higher concentrations.

CONCLUSIONS

We have successfully utilized the LbL technique to fabricate nanocomposite thin film of TiO_2 nanoparticles, CPANI and PSS. The CPANI containing films show better catalytic activity than the films without CPANI layers for both anionic and cationic dyes. The dye adsorption property of CPANI enhances the degradation of dye by bringing dye molecules more effectively to the catalytic site. The adsorption property of one component (CPANI) enhances the photodegradation property of other component (TiO_2) in a catalytic film deposited by LbL approach. Thus in this paper, we have demonstrated that LbL self-assembly of nanocomposites may be used as an alternative approach for the effective photodegradation of textile dyes.

Acknowledgment. We thank the Department of Science and Technology, India, for financial support. The authors thank the Institute Nanoscience center for SEM images.

Supporting Information Available: FTIR, ^{1}H NMR of CPANI, and degradation profiles of Orange G and Rhodamine B with different number of catalytic slides of CPANI/PSS/TiO_2 nanoparticles (PDF). This material is available free of charge via the Internet at http://pubs.acs.org.

REFERENCES AND NOTES

(1) Chu, W. *Wat. Res.* **2001**, *35*, 3147.
(2) Neppolian, B.; Choi, H. C.; Sakthivel, S.; Arabindoo, B.; Murugesan, V. *Chemophore* **2002**, *46*, 1173.
(3) Chakrabarti, S.; Dutta, B. K. *J. Hazard. Mater.* **2004**, *B112*, 269.
(4) Kansal, S. K.; Singh, M.; Sud, D. *J. Hazard. Mater.* **2007**, *141*, 581.
(5) McKay, G.; Blair, H. S.; Gardner, J. R. *J. Appl. Polym. Sci.* **1982**, *27*, 3043.
(6) Annadurai, G.; Juang, R. S.; Lee, D. J. *J. Hazard. Mater.* **2002**, *B92*, 263.
(7) Namasivayam, C.; Kavitha, D. *Dyes Pigm.* **2002**, *54*, 47.
(8) Al-Bastaki, N. *Chem. Eng. Process.* **2004**, *43*, 1561.
(9) Golob, V.; Vinder, A.; Simonic, M. *Dyes Pigm.* **2005**, *67*, 93.
(10) Mahanta, D.; Madras, G.; Radhakrishnan, S.; Patil, S. *J. Phys. Chem. B* **2008**, *112*, 10153.
(11) Mahanta, D.; Madras, G.; Radhakrishnan, S.; Patil, S. *J. Phys. Chem. B* **2009**, *113*, 2293.
(12) Linsebigler, A. L.; Lu, G.; Yates, J. T. *Chem. Rev.* **1995**, *95*, 735.
(13) Yang, J. L.; An, S. J.; Park, W.; Yi, G. C.; Choi, W. *Adv. Mater.* **2004**, *16*, 1661.
(14) Chang, H. T.; Wu, N. M.; Zhu, F. *Wat. Res.* **2000**, *34*, 407.
(15) Arabatzis, T. M.; Antonaraki, S.; Stergiopoulos, T.; Hiskia, A.; Papaconstantinou, E.; Bernard, M. C.; Falaras, P. *J. Photochem. Photobiol. A* **2002**, *149*, 237.
(16) Hammond, P. T. *Curr. Opin. Colloid Interface Sci.* **2000**, *4*, 430.
(17) Decher, G. *Science* **1997**, *277*, 1232.
(18) Manna, U.; Patil, S. *ACS Appl. Mater. Interfaces* **2010**, *2*, 1521.
(19) Manna, U.; Patil, S. *J. Phys. Chem. B* **2009**, *113*, 9137.
(20) Manna, U.; Patil, S. *J. Phys. Chem. B* **2008**, *112*, 13258.
(21) Khopade, A. J.; Caruso, F. *Nano Lett.* **2002**, *2*, 415.
(22) Caruso, R. A.; Susha, A.; Caruso, F. *Chem. Mater.* **2001**, *13*, 400.
(23) Decher, G.; Hong, J. D. *Makromol. Chem. Macromol. Symp.* **1991**, *46*, 321.
(24) Manna, U.; Bharani, S.; Patil, S. *Biomacromolecules* **2009**, *10*, 2632.
(25) Manna, U.; Dhar, J.; Nayak, R.; Patil, S. *Chem Comm.* **2010**, *46*, 2250.
(26) Sohn, B. H.; Kim, T.-H.; Char, K. *Langmuir* **2002**, *18*, 7770.
(27) He, J.-A.; Mosurkal, R.; Samuelson, L. A.; Li, L.; Kumar, J. *Langmuir* **2003**, *19*, 2169.
(28) Kniprath, R.; Duhm, S.; Glowatzki, H.; Koch, N.; Rogaschewski, S.; Rabe, J. P.; Kirstein, S. *Langmuir* **2007**, *23*, 9860.
(29) Priya, D. N.; Modak, J. M.; Raichur, A. M. *ACS Appl. Mater. Interfaces* **2009**, *1*, 2684.
(30) Cheung, J. H.; Stockton, W. B.; Rubner, M. F. *Macromolecules* **1997**, *30*, 2712.
(31) Stockton, W. B.; Rubner, M. F. *Macromolecules* **1997**, *30*, 2717.
(32) Annaduri, G.; Ling, L. Y.; Lee, G. W. *J. Hazard. Mater* **2008**, *152*, 337.
(33) MacDiarmid, A. G.; Chiang, J. C.; Richter, A. F.; Somasiri, N. L. D.; Epstein, A. J. In *Conducting Polymers*; Alcacer, L., Ed.; Reidel: Dordrecht, The Netherlands, 1987, 105.
(34) Yang, S.; Tirmizi, S. A.; Burns, A.; Barney, A. A.; Risen, W. M. *Synth. Met.* **1989**, *32*, 191.
(35) Yavuz, A. G.; Uygun, A.; Bhethanabotla, V. R. *Carbohy. Polym.* **2009**, *75*, 448.
(36) Ismail, Y. A.; Shin, S. R.; Shin, K. M.; Yoon, S. G.; Shon, K.; Kim, S. I.; Kim, S. J. *Sens. Actuators, B* **2008**, *129*, 834.
(37) Che, A.-F.; Liu, Z.-M.; Huang, X.-J.; Wang, Z.-G.; Xu, Z.-K. *Biomacromolecules* **2008**, *9*, 3397.
(38) Wei, X.-L.; Wang, Y. Z.; Long, S. M.; Bobeczko, C.; Epstein, A. J. *J. Am. Chem. Soc.* **1996**, *118*, 2545.
(39) Trchova, M.; Stejskal, J.; Prokes, J. *Synth. Met.* **1999**, *101*, 840.
(40) Marcasuzaa, P.; Reynaud, S.; Ehrenfeld, F.; Khoukh, A.; Desbrieres, J. *Biomacromolecules* **2010**, *11*, 1684.
(41) Monkman, A. P.; Bloor, D.; Stevens, G. C.; Stevens, J. C. H.; Wilson, P. *Synth. Met.* **1989**, *29*, E277.
(42) Hejazi, R.; Amiji, M. *J. Controlled Release* **2003**, *89*, 151.
(43) Chowdhury, A. N.; Jesmeen, S. R.; Hossain, M. M. *Polym. Adv. Technol.* **2004**, *15*, 633.
(44) Ayad, M. M.; El-Nasr, A. A. *J. Phys. Chem. C* **2010**, *114*, 14377.
(45) Zhang, H.; Zong, R.; Zhoa, J.; Zhu, Y. *Environ. Sci. Technol.* **2008**, *42*, 3803.

AM1009265